Field-induced reorientation of the spin helix in MnSi near T_c

S. V. Grigoriev,[1,*] S. V. Maleyev,[1] A. I. Okorokov,[1] Yu. O. Chetverikov,[1] and H. Eckerlebe[2]
[1]*Petersburg Nuclear Physics Institute, Gatchina, St. Petersburg 188300, Russia*
[2]*GKSS Forschungszentrum, 21502 Geesthacht, Germany*

(Received 6 February 2006; revised manuscript received 20 April 2006; published 28 June 2006)

The chiral spin fluctuations and the spiral structure of the single crystal MnSi has been studied by small angle polarized neutron scattering near $T_c=29$ K under applied field. A weak magnetic field applied along one of the $\langle 111\rangle$ axes produces a single domain sample with the helix wave vector along the field. The 90° reorientation of the spin spiral from the [111] axis to $[1\bar{1}0]$ axis is observed in the field range from 130 to 180 mT in the close vicinity to T_c. Further increase of the field above 180 mT restores the original orientation of the helix and leads to the induced ferromagnetic state at 350 mT. This observation clarifies the nature of the structural spin instability found in the *H-T* phase diagram of MnSi by other techniques. We explain this phenomenon as a result of competition of cubic anisotropy and the spin-wave Bose condensation provoked by the field perpendicular to the helix axis.

DOI: 10.1103/PhysRevB.73.224440 PACS number(s): 75.40.−s, 61.12.Ex

I. INTRODUCTION

The weak itinerant cubic helimagnet MnSi with the space group $P2_13$ and the lattice constant $a=4.558$ Å orders below $T_c=29$ K in a left-handed spiral along the $\langle 111\rangle$ directions with a propagation vector $\mathbf{k}=(2\pi/a)(\xi,\xi,\xi)$, where $\xi=0.017$.[1,2] Its helicity is a result of antisymmetric Dzyaloshinski-Moriya (DM) exchange interaction caused by the lack of a center of symmetry in Mn atomic arrangement.[3–6] This DM interaction is isotropic itself but another more weak anisotropic exchange (AE) interaction fixes a direction of the magnetic spiral along one of the cube diagonals.[4]

The magnetic properties of MnSi has attracted much attention in recent years because of the discovery of the quantum phase transition (QPT) to magnetically disordered state, which is easily reached under applied pressure. As was found in Refs. 7–9 the magnetic transition temperature T_c decreases with increasing pressure and the magnetic order disappears at $T=0$ and the critical pressure of $P_c\approx 14.6$ kbar. Below $P^*\approx 12$ kbar the temperature transition is of the second order, while above P^* it is weakly of the first order. Close to the QPT the temperature dependent part of the electrical resistance shows deviations from Fermi liquid behavior with $\Delta\rho=AT^{3/2}$ over a wide temperature range.[8] This finding supports the existence of novel metallic phases with partial ordering of the conduction electrons as proposed for the high temperature superconductors[10] and heavy-fermion compounds.[11] The QPTs are driven by quantum fluctuations. Accounting for the fact that the applied critical pressure changes the value of the effective moment insignificantly[12] one has to suppose that the magnetic system is close to a ferromagnetic instability. Up to now the origin of this instability is unclear.

The magnetic behavior of MnSi under applied magnetic field remains also puzzling. It is believed that at $T\ll T_c$ the magnetic spiral domains transform into a single domain in a weak magnetic field H_{c1} of order of 70 mT and a conical phase appears.[1,2] The cone angle decreases as the field increases and the induced ferromagnetic state appears at $H_{c2}\approx 600$ mT with the saturated magnetic moment of $0.4\mu_B$ per Mn atom. This value of the moment is much smaller than the effective paramagnetic moment above T_c, which has been estimated to be $1.4\mu_B$ from the susceptibility measurements.[1] It is shown also that the helix wave vector $\mathbf{k}$ rotates toward the direction of the field if initially it is not collinear to a cubic diagonal. The period of the spiral does not depend on the field direction.[1] The helix rotation was theoretically considered by Plumer and Walker on the base of the phenomenological approach.[13,14] However, the reorientation process has not been well understood. It is only recently the microscopic origin of this effect was clarified by the consideration, which takes into account the cubic anisotropy, Zeeman energy and the spin-wave condensation provoked by the field component perpendicular to the helix axis.[15] In particular this theory allows one to explain appearance of the second harmonic of the helix structure, which was observed in weak perpendicular field.[16,17]

The situation becomes even more complicated near T_c. In zero field the critical behavior of the MnSi was recently studied by small angle scattering of polarized neutrons.[18] As was shown in Ref. 18 the spiral structure above T_c transforms into chiral spin fluctuations with the spiral period close to the period of the helix below T_c (16 nm). The correlation length of these fluctuations diverges along $\langle 111\rangle$ axes only as $R_c\sim(\tau^{-\nu})$ with the corresponding critical exponent $\nu=0.62(1)$. These results are in a qualitative agreement with the mean-field calculations based on the Bak-Jensen model that takes into account the exchange interaction, the isotropic DM interaction and the weak AE interaction.[18]

In the magnetic field a new, so-called, *A* phase was found at $H_A\sim 200$ mT and slightly below T_c by measuring the magnetization and magnetoresistance.[19] The neutron scattering experiments had shown that the intensity of the helical Bragg reflection decreased strongly in the narrow range of $H\sim H_A$ near T_c.[20] This was interpreted as a new paramagnetic phase just below T_c provoked by the field. The ac susceptibility measurements under applied pressure has confirmed the presence of the *A* phase near T_c in the field range from H_{A1} to H_{A2}.[21] It was also found that while T_c drops rapidly with increase of pressure, absolute values of the characteristic fields H_{c1}, H_{c2} and H_{A1}, H_{A2} change insignificantly.

On the other hand, the anomaly in ac susceptibility associated with the A phase disappears altogether as soon as P approaches P^*. Thus, one may suppose that the A phase is connected to the change of the kind of the transition from the second order below P^* to the weakly first order above P^*. It is also recognized that the presence of the A phase could be explained by none of the existing theories.

In this paper we study the nature of this instability of the helix structure by polarized small angle neutron scattering (SANS) and propose an explanation of its origin. The paper is organized in the following way. Section II gives a description of the theoretical and experimental background. The expressions are given describing the neutron scattering from the spin fluctuations near T_c and Bragg reflections from the helix structure below T_c. Experimental details of the method used are presented as well. In Sec. III we present results of the SANS study of both critical fluctuations and ordered magnetic structure in MnSi under applied field and at ambient pressure. The 90° reorientation of the spin spiral from the [111] axis to $[1\bar{1}0]$ axis is observed in the magnetic field ranging from 130 to 180 mT in the close vicinity to T_c. Thus we show that the helix 90° rotation occurs but not a new paramagnetic phase. The data analysis is given in Sec. IV. In Sec. V we explain the obtained results using theory of Ref. 15. It is shown that 90° reorientation of the helix axis happens due to mutual interplay of the AE interaction and cubic anisotropy in presence of the perpendicular magnetic field, which leads to Bose condensation of the spin waves and additional negative contribution to the free energy. The explanation implies the existence of the spin wave gap, which originates from the cubic anisotropy and the interaction between spin waves.[15] The gap stabilizes the spin structure of MnSi with respect to the small magnetic field perpendicular to the helix wave vector. We speculate that the applied pressure changes the strength of the cubic anisotropy that makes the gap negative. Therefore, the spin structure becomes intrinsically unstable which inevitably leads to the QPT from ordered to the spin liquid state. The conclusion is given in Sec. VI.

II. THEORETICAL AND EXPERIMENTAL BACKGROUND

The magnetic structure of MnSi was explained assuming the hierarchy of the interactions: the conventional isotropic exchange, the isotropic DM interaction, and the weak anisotropic exchange with characteristic energies B, Da, and F, respectively. The energies Da and F are of the first and second order in the spin-orbit interaction, so that $B > Da > F$. According to Refs. 3 and 4 an interplay of these interactions results in the appearance of the single helix structure with the wave vector $k = |D|/B$. The handedness of the helicity is determined by the sign of the DM interaction. The direction of $\mathbf{k}$ is fixed by the weak anisotropic exchange $[|F|/(2B) = U \ll 1]$. If $F < 0$ then the spiral is directed along the cube diagonals $\langle 111 \rangle$ (MnSi case) while at $F > 0$ it is along one of the cubic edges $\langle 100 \rangle$ (FeGe case for high temperature phase[16]).

According to Ref. 15 the simple helical structure in the magnetic field $H_{\|k}$ along the helix axis $\mathbf{k}$ is described by

$$\mathbf{S}_R = \hat{c} \sin\alpha + [\mathbf{A} e^{i\mathbf{k}\cdot\mathbf{R}} + \mathbf{A}^* e^{-i\mathbf{k}\cdot\mathbf{R}}] \cos\alpha, \tag{1}$$

where $\mathbf{S}_R$ is the spin of the unit cell, $\mathbf{A} = (\hat{a} - i\hat{b})/2$, $\hat{a}$, $\hat{b}$, and $\hat{c}$ are mutually orthogonal unit vectors ($\hat{c} = [\hat{a} \times \hat{b}]$), and

$$\sin\alpha = -H_{\|}/H_{c2}, \tag{2}$$

where H_{c2} is the field of the transition to the field induced ferromagnetic state. This expression correctly describes the helical structure of MnSi if $\hat{c}$ and the wave vector of the helix $\mathbf{k}$ are antiparallel (left-hand helix) (see Ref. 4 and references therein). The neutron elastic cross section on the magnetic helix below T_c normalized on the unit cell has the following form:[22,23]

$$\frac{d\sigma}{d\Omega} = \left(\frac{rS}{2}\right)^2 \frac{(2\pi)^3}{V_0} [1 + (\hat{q}\hat{c})^2 - 2(\hat{q}\mathbf{P}_0)(\hat{q}\hat{c})] \sin^2\alpha \, \delta(\mathbf{q} - \mathbf{k}), \tag{3}$$

where $r = 0.54 \times 10^{-12}$ cm, V_0 is the unit cell volume, and $\delta(\mathbf{q} - \mathbf{k})$ provides the Bragg conditions are fulfilled. For the single-handed helical structure the cross-section depends on the incident neutron polarization $\mathbf{P}_0$. When $\mathbf{P}_0$ is along $\hat{c}$, the scattering is forbidden at $\mathbf{q} = \mathbf{k}$ but if $\mathbf{P}_0$ is antiparallel to $\hat{c}$, it is maximal. If $\mathbf{P}_0 \perp \hat{\mathbf{c}}$, the scattering does not depend on the polarization. In arbitrary case the polarization of the neutron scattering is determined as $P = [\sigma(\mathbf{P}_0) - \sigma(-\mathbf{P}_0)]/[\sigma(\mathbf{P}_0) - \sigma(-\mathbf{P}_0)]$, and accounting for Eq. (3) may be written $P = (\hat{q}\mathbf{P}_0) = \cos\phi$ where ϕ is the angle between the incident polarization and the scattering vector. This equation holds for all measurements presented below at $T < T_c$.

For the paramagnetic phase ($T > T_c$) the neutron cross section on the helix spin fluctuations in the mean field approximation is given by[18]

$$\frac{d\sigma}{d\Omega} = r^2 \frac{T}{B[(q+k)^2 + \kappa^2]} \times \frac{k^2 + \kappa^2 + q^2 + 2\dfrac{D}{|D|} k\mathbf{q}\cdot\mathbf{P}_0}{(q-k)^2 + \kappa^2 + k^2 U(\hat{q}_x^4 + \hat{q}_y^4 + \hat{q}_z^4 - 1/3)}. \tag{4}$$

Here κ is the inverse correlation length of the spin fluctuations, $\mathbf{q}$ is the scattering vector, and $\hat{q} = (\hat{q}_x, \hat{q}_y, \hat{q}_z) = \mathbf{q}/|q|$. This expression catches the main symmetry features of the problem and takes into account all interactions mentioned above. We note also that in MnSi the ratio $D/|D| = -1$. It corresponds to the left-handed helix below T_c.

Remarkable features of this expression follow.

(i) This function is maximal at $|\mathbf{q}| = k = |D|/B$, it is a result of the DM interaction. If we neglect the small U term in the denominator then the scattering intensity for unpolarized neutrons is a constant value along the ring with the radius k around the incident beam with the width of order of κ.

(ii) For completely polarized neutrons ($|\mathbf{P}_0| = 1$) the scattering intensity depends on the mutual orientation of the vectors $\mathbf{q}$ and $\mathbf{P}_0$. If $\mathbf{P}_0 \uparrow \downarrow \mathbf{q}$, the scattering is maximal at the ring $|q| = k$ and is equal to $r^2(T/B)(k/\kappa^2)$. If $\mathbf{P}_0 \uparrow \uparrow \mathbf{q}$, the scattering intensity is minimal. Thus for polarized neutrons the scattering looks like half of the ring with maximal intensity

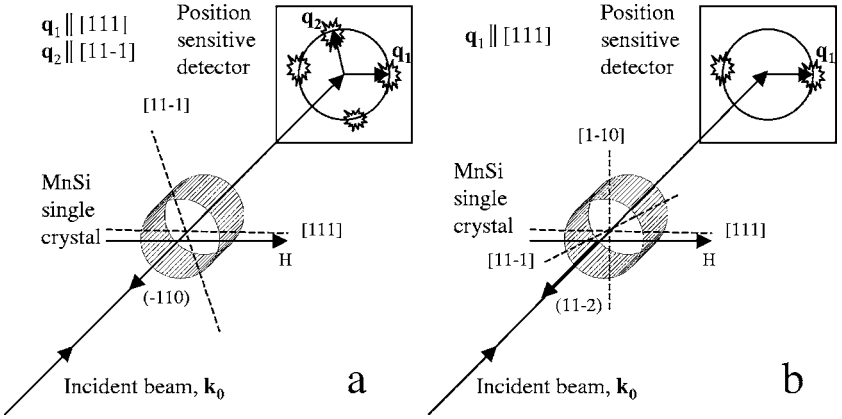

FIG. 1. The schematic outline of SANS experiment. The single crystal MnSi was oriented such that the incident beam heated the sample along two different crystallographic axes of interest. (a) Orientation (i): with the beam along the $[1\bar{1}0]$ axis and (b) orientation (ii) with the beam along the $[11\bar{2}]$ axis. The magnetic field $\vec{H}$ and the polarization **P** was set along to the [111] axis.

at $\mathbf{P}_0 \uparrow \downarrow \mathbf{q}$. The polarization of the scattering is written as[18] $P = 2\kappa q P_0 \cos\phi/(q^2+k^2+\kappa^2)$. This expression describes well the polarization experimentally detected above T_c for all measurements presented below.

(iii) The small U term in the denominator is proportional to the cubic invariant $\hat{q}_x^4+\hat{q}_y^4+\hat{q}_z^4-1/3$. As a result the scattering intensity depends on the orientation of the vector **q** relative the cubic axes. As $U \ll 1$ this dependence appears in the very vicinity to T_c where κ^2 becomes very small. This effect is solely determined by the very weak anisotropic exchange. In the case of MnSi the $\langle 111 \rangle$ is the easy direction. The scattering along it is maximal and the renormalized inverse correlation length diverges as $T \to T_c$. At the same time the $\langle 100 \rangle$ direction is the hard one and the correlation length remains finite.[18]

The single crystal MnSi was chosen for the study. The sample was a disc with a thickness of 1.5 mm and a diameter of 15 mm. The crystallographic mosaicity and orientation of the sample was tested on the x-ray diffractometer at GKSS (Germany). The average value of the full width at half maximum (FWHM) over all measured reflections is 0.25°. The polarized SANS experiments were carried out at the SANS-2 scattering facility of the FRG-1 research reactor in Geesthacht (Germany). A polarized beam of neutrons with an initial polarization of $P_0=0.95$, the neutron wavelength $\lambda = 0.58$ nm ($\Delta\lambda/\lambda = 0.1$) and a divergence of 2.5 mrad was used. The scattered neutrons were detected by a position sensitive detector with 256×256 pixels. The detector-sample distance was set such that the q range was covered from 6×10^{-2} to 1 nm^{-1} with a step of 0.01 nm^{-1}.

Our goal is to study possible reorientation of the helix vector **k** in magnetic field applied along [111] direction. For this purpose we have used two configurations with the neutron wave vector $\mathbf{k}_0$ directed along the $[\bar{1}10]$ axis (i) and along the $[11\bar{2}]$ axis (ii) shown in Figs. 1(a) and 1(b), respectively. In these two cases we can study different Bragg reflections, which lay in two different scattering planes perpendicular to the beam. In the first (i) case [Fig. 1(a)] Bragg reflections with **k** parallel to [111], $[1\bar{1}1]$, [110], and [001] may be observed. The second (ii) configuration [Fig. 1(b)] allows one to detect reflections along the [111] and $[1\bar{1}0]$ axes.

It is important to note that if the field is applied parallel to the [111] axis then the three other $\langle 111 \rangle$ axes as well as three $\langle 100 \rangle$ axes are equivalent with respect to the field. On the contrary, the axes [110], [101], and [011], which are inclined for about 35° to the field direction [configuration (i), Fig. 1(a)], are not equivalent to $[1\bar{1}0]$, $[10\bar{1}]$, and $[01\bar{1}]$, which are perpendicular to the field [configuration (ii), Fig. 1(b)]. Therefore, at least two different orientations of the crystal are needed to complete a picture of the reorientation process of the spin helix under applied field.

III. MEASUREMENTS

We have used the field ranged from 0 to 800 mT and directed along [111] axis. The scattering intensity was measured in the temperature range from $T=25$ to 50 K with accuracy better than 0.02 K. The helix spin structure of MnSi were studied both above and below T_c under applied field. Maps of the SANS intensities below T_c are shown in Fig. 2 for two different orientations of the MnSi crystal and for four values of the magnetic field. For orientation (i) ($\mathbf{k}_0 \| [1\bar{1}0]$) and in zero field [Fig. 2(a), left column] four Bragg peaks, reflections from the domains oriented along [111] and $[11\bar{1}]$, with $k=0.39$ nm^{-1} are visible. This is possible due to the large magnetic mosaic, as in ideal case the Bragg condition would be only fulfilled for one reflection. For orientation (ii) ($\mathbf{k}_0 \| [11\bar{2}]$) and in the zero field [Fig. 2(a), right column] two reflections from the domains oriented along [111] are observed.

When the magnetic field $H > H_{c1}$ is applied along the [111] axis, we get a single domain sample as the reflections corresponding to $[11\bar{1}]$ reflection disappear and intensity of the [111] reflection increases [see Fig. 2(b), both the left and right columns]. Stronger magnetic field $H \simeq 150$ mT applied along [111] axis results in a collapse of the spiral structure along [111] [Fig. 2(c)] and in appearance of the reflections along $[1\bar{1}0]$ [Fig. 2(c), right column]. With further increase of the field above 180 mT the helix structure along [111] restores and the $[1\bar{1}0]$ reflection vanishes. At $H=H_{c2} \simeq 350$ mT the helix transforms into the induced ferromagnet and the Bragg reflections dissolve.

The similar picture, but less pronounced, is observed for the critical scattering above T_c. In zero field the diffuse scattering intensity looks similar to a ring with the maximum at $q \simeq k$ [Fig. 3(a)]. There are weak spots on the ring (outlined

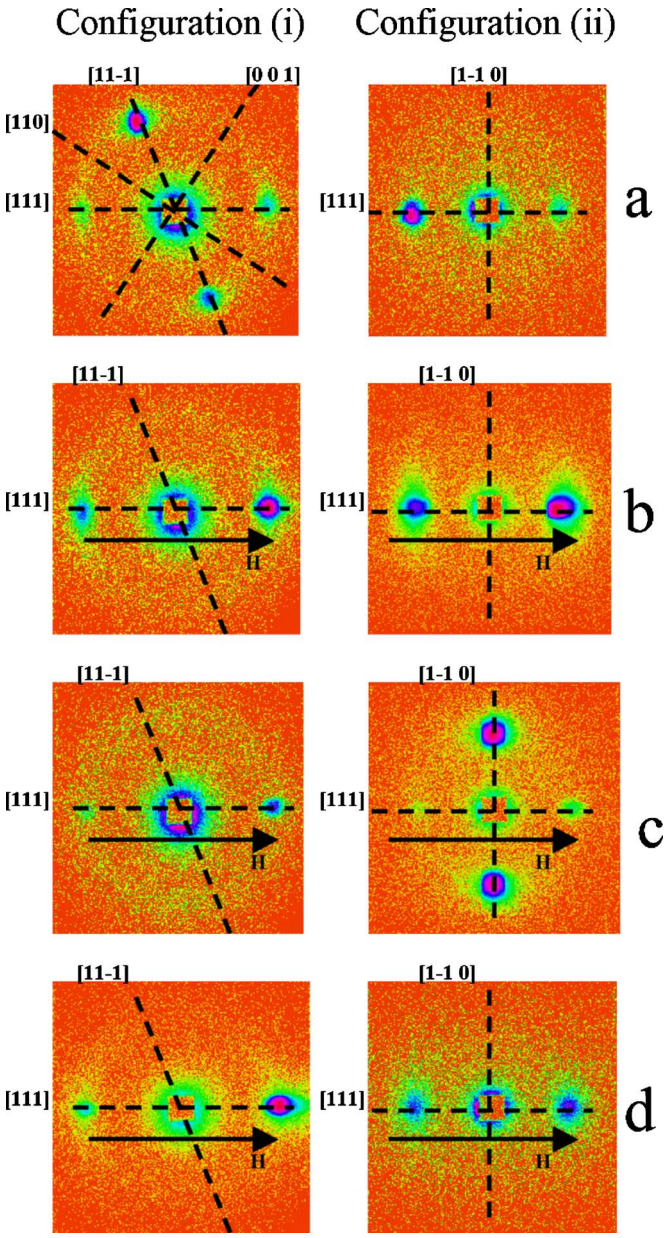

FIG. 2. (Color online) Maps of the SANS intensities for $T=T_c-0.2\approx 28.5$ K for two different orientations of the MnSi crystal. Left column: orientation (i) ($\mathbf{k}_0\|[1\bar{1}0]$) and right column: orientation (ii) ($\mathbf{k}_0\|[11\bar{2}]$) and for four values of the magnetic field: (a) $H=0$, (b) $H=80$ mT, (c) $H=150$ mT, and (d) $H=220$ mT.

in Fig. 3 by dashed contours), which below T_c transform into the Bragg peaks originating from the helical structure. The origin of these spots was explained in Ref. 18. The ring is observed in the temperature range from 1 K below T_c to 1 K above T_c. This suggests that the ring is induced by the critical fluctuations. When the magnetic field is applied along the [111] axis [Fig. 3(b)], it strengthens two spots associated to the [111] axis. Note that such field does not affect the intensity of the ring. Further increase of the field produces the same effect as described for the helix structure below T_c: first, weak spots appear along $[1\bar{1}0]$ axis while spots along [111] weaken at $H\sim 150$ mT [Fig. 3(c)]; then the scattering

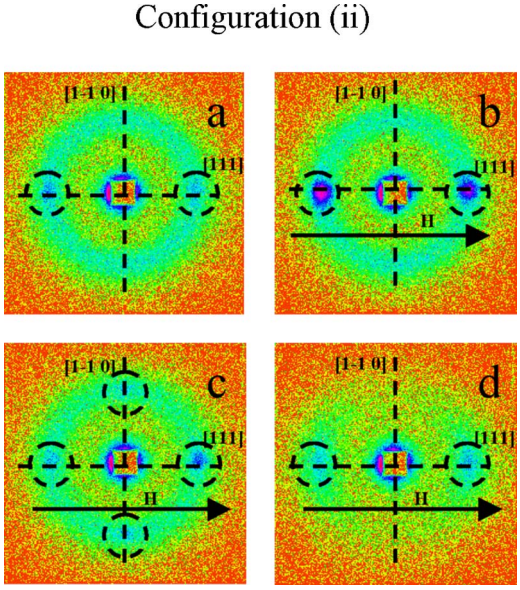

FIG. 3. (Color online) Maps of the SANS intensities for $T=T_c+0.3\approx 29.0$ K for orientation (ii) ($\mathbf{k}_0\|[11\bar{2}]$) and for four values of the magnetic field: (a) $H=0$, (b) $H=80$ mT, (c) $H=150$ mT, and (d) $H=220$ mT. For better visibility weak spots on the ring are outlined by dashed contours.

along $[1\bar{1}0]$ axis vanishes but spots along [111] remain at $H\sim 220$ mT [Fig. 3(d)].

Thus, we observe the 90° reorientation of the spin helix from the [111] axis to $[1\bar{1}0]$ axis under magnetic field $H\sim 150$ mT applied along [111] in the close vicinity to T_c. The details of the reorientation process are presented below in the data analysis of the temperature and magnetic field scans for two different sample orientations.

IV. DATA ANALYSIS

A. Zero field temperature scan

The zero field temperature evolution of the neutron scattering in the critical range was discussed in details in Ref. 18. The present data confirm the experimental findings and theoretical description of the previous work. In particular, the critical scattering is arranged as a ring centered at $|q|=0$ with the radius of $k=0.40$ nm^{-1}. For configuration (i) the temperature dependence of the scattering intensity at $|q|=k$, or intensity of the ring, is shown in Fig. 4 for **q** parallel to [111] axis (easy direction) and **q** parallel to [001] direction (hard direction). The critical temperature is found to be $T_c=28.75\pm 0.05$ K. The intensity of the ring increases with decreasing temperature both along the [111] and [001] axes. Close to T_c the intensity along the [001] axis saturates while the intensity along the [111] axis continues to increase, thus, forming spots on the ring. With further lowering temperature below T_c the spots on the ring transform into Bragg reflections along the [111] axes but intensity of the ring in the [001] direction decreases. As in Ref. 18 we argue that the anisotropic exchange interaction plays a significant role in the close vicinity to T_c. This leads to the difference in the

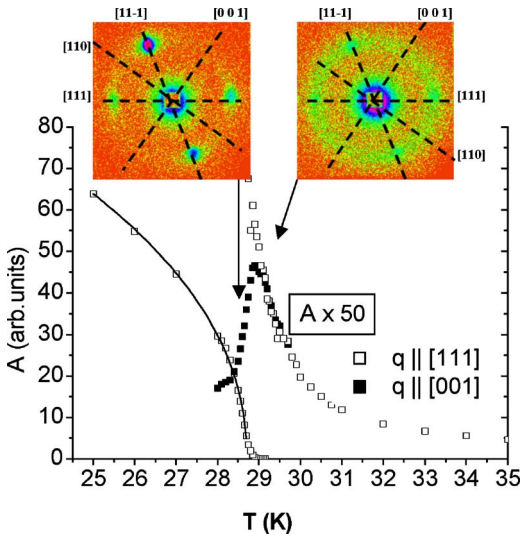

FIG. 4. (Color online) The scattering intensity at $|q|=k$ in the easy ([111]) and hard ([001]) directions as a function of temperature at $H=1$ mT. Intensity is increased by factor 50 at $T>T_c$. Two insets show maps of the scattering intensity [configuration (i)] for $T<T_c$ and $T>T_c$, respectively.

intensity of the ring along [111] and [001] directions as T approaches T_c.

The longitudinal q scans along different directions across the ring shows that the ring intensity is well described by the Lorentzian for all the data above T_c and for the scan along the hard direction below T_c. The scans for the Bragg reflections, i.e., along the easy axes $\langle 111\rangle$ below T_c, are described by the Gaussian with the constant HWHM corresponding to the resolution of the experimental setup. The q dependence of the scattering intensity above T_c was fitted to Eq. (4) for $\mathbf{q}$ along the [111] and [001] axes. The parameters $A=r^2(T/B)$ and $\kappa_{e,h}$ have been obtained from the fit. The inverse correlation length $\kappa_{e,h}$ along the "easy" and "hard" directions is presented in Fig. 5 as a function of the reduced temperature $\tau=(T-T_c)/T_c$. It is well seen that the system becomes anisotropic at $\tau<0.03$. The parameter κ_e is well described by the scaling law $\kappa=\kappa_0\tau^\nu$ with $\nu=0.68(3)$ and $\kappa_0=1.5$ nm^{-1}. As a result the correlation length diverges along $\langle 111\rangle$ directions only.

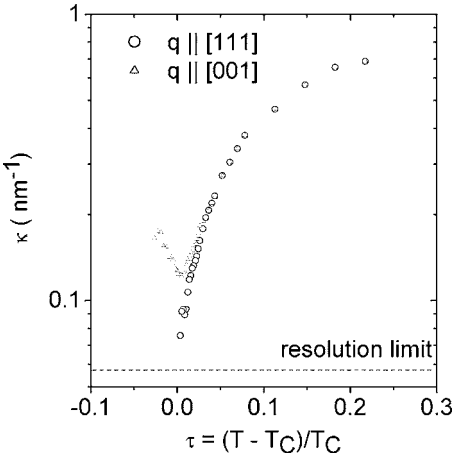

FIG. 5. τ dependence of the inverse correlation length for the easy $\mathbf{q}\|(111)\|H$ and hard $\mathbf{q}\|[001]$ directions.

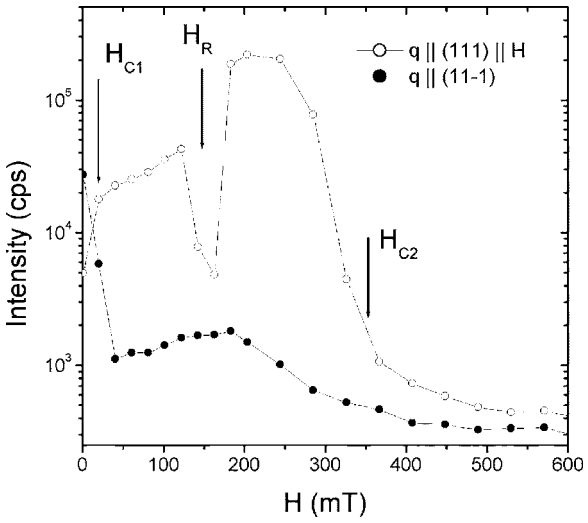

FIG. 6. Configuration (i) ($\mathbf{k}_0\|[1\bar{1}0]$). Magnetic-field dependence of the Bragg intensity for $\mathbf{q}\|(111)\|H$ and $\mathbf{q}\|(11\bar{1})$ at $T=T_c-0.2=28.5$ K.

B. Magnetic field scan below T_c

The magnetic field dependence of the scattering intensity was measured below T_c for the configuration (i) ($\mathbf{k_0}\|[\mathbf{1\bar{1}0}]$) [Fig. 1(a)] and configuration (ii) ($\mathbf{k_0}\|[\mathbf{11\bar{2}}]$) [Fig. 1(b)]. Figures 6 and 7 show the Bragg intensity measured at $T=T_c-0.2=28.5$ K along the [111] and $[11\bar{1}]$ axes for configuration (i) and along the [111] and $[1\bar{1}0]$ axes for configuration (ii), respectively. The intensity of the [111] reflex increases in the field while the reflection at $[11\bar{1}]$ disappears at $H\leq H_{c1}$. Thus we observe the reorientation of all helical domains toward the only [111] axis, which is parallel to the applied field. The intensity of the [111] reflection increases smoothly at $H>H_{c1}$ but it has a drastic feature at $H\simeq 150$ mT, showing a "collapse" of the spiral structure along the [111] axis

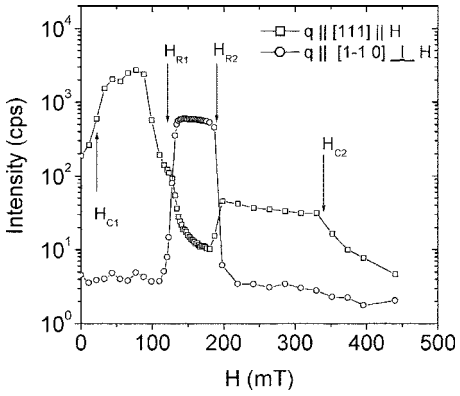

FIG. 7. Configuration (ii) ($\mathbf{k}_0\|[11\bar{2}]$). Magnetic-field dependence of the Bragg intensity for $\mathbf{q}\|(111)\|H$ and $\mathbf{q}\|(1\bar{1}0)$ at $T=T_c-0.2=28.5$ K.

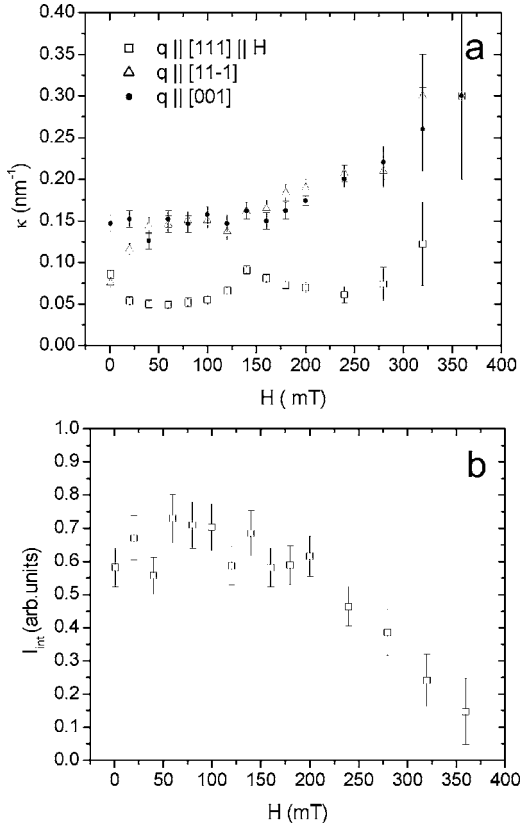

FIG. 8. Configuration (i) ($\mathbf{k}_0 \| [1\bar{1}0]$). Magnetic-field dependence of the inverse correlation length for $\mathbf{q} \| (111) \| H$, $\mathbf{q} \| [11\bar{1}]$, and $\mathbf{q} \| [001]$ (a) and the integral intensity of the scattering at $T = T_c + 0.2$ K.

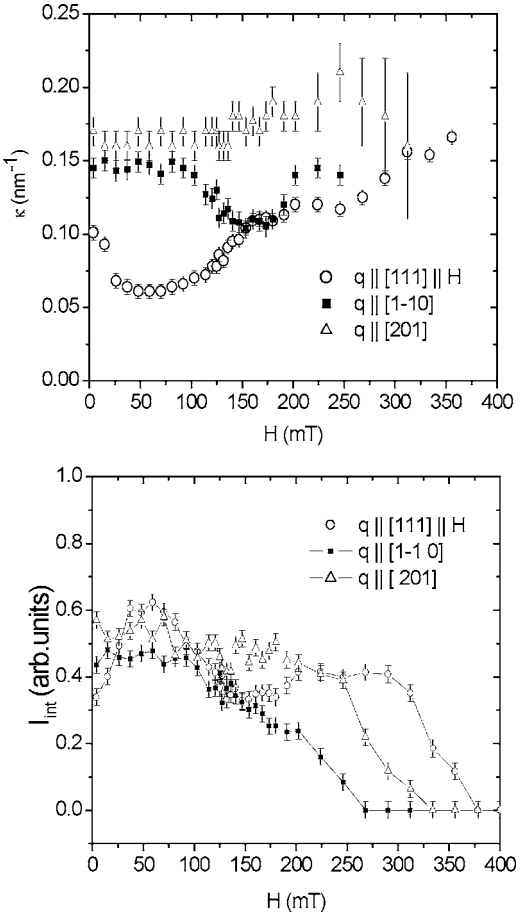

FIG. 9. Configuration (ii) ($\mathbf{k}_0 \| [11\bar{2}]$). Magnetic-field dependence of the inverse correlation length (a) and the integral intensity of the scattering for $\mathbf{q} \| [111] \| H$, $\mathbf{q} \| [1\bar{1}0]$, and $\mathbf{q} \| [201]$ at $T = T_c + 0.2$ K.

(Figs. 6 and 7). Instead, the Bragg reflection $(1\bar{1}0)$ arises and remains constant within the range $130 < H < 180$ mT (Fig. 7). Therefore, the "collapse" of the helix structure is explained by the rotation of the helix wave vector $\mathbf{k}$ from the direction parallel to the field $\mathbf{k} \| [\mathbf{111}] \| \mathbf{H}$ to the direction perpendicular to the field $\mathbf{k} \| [\mathbf{1\bar{1}0}] \perp \mathbf{H}$. No real "collapse" takes place and no real new phase, a so-called A phase, occurs.

With further increase of the field the spiral structure reappears again in $[111]$ direction and dissolves in the $[1\bar{1}0]$ direction. At $H = H_{c2} \simeq 360$ mT the intensity of the Bragg reflections decreases to the background level. This implies transformation from the helical to ferromagnetic structure. As to the $[11\bar{1}]$ axis (Fig. 6), a weak critical-like scattering is still observed at the place of the former Bragg peak. The intensity of this scattering is maximal at $H \sim 150$ mT. It should be noticed that the q scan along $[111]$ direction is well fitted by the Gaussian. This shape remains a Gaussian-type at $H \sim 150$ mT which implies the partial rather than full disorder of the spiral at this field.

C. Magnetic field scan above T_c

The scattering intensity was measured as a function of the field above T_c for configuration (i) ($\mathbf{k}_0 \| [1\bar{1}0]$) (Fig. 8) and configuration (ii) ($\mathbf{k}_0 \| [11\bar{2}]$) (Fig. 9). q scans along $[111]$, $[11\bar{1}]$, and $[001]$ axes are well described by the Lorentzian centered at $q = k$ with the width κ and the amplitude A.

For configuration (i) ($\mathbf{k}_0 \| [1\bar{1}0]$) the parameters obtained from the fit, the inverse correlation length κ and the integral intensity of the peak I_{int} are shown in Figs. 8(a) and 8(b), respectively, at $T = T_c + 0.2$ K. As seen from Fig. 8(a), the inverse correlation length κ for $\mathbf{q} \| [001]$ does not change significantly with the magnetic field. For $\mathbf{q} \| [11\bar{1}]$ its value increases at $H < H_{c1} = 40$ mT and practically coincides with that along $[001]$ axis at $H > H_{c1}$. This means that the magnetic field, applied along $[111]$ axis, eliminates an effect of the AE interaction to the critical fluctuations along the direction of $[11\bar{1}]$ axis. It is interesting to note that the values of H_{c1} below and above T_c are close to each other and equal 30 mT. The remarkable change of κ with the applied field is observed for $\mathbf{q} \| \mathbf{H} \| [111]$. First κ decreases to the resolution level at $H = H_{c1}$, then it increases again at $H = H_{c2} \approx 350$ mT, having a well-pronounced intermediate maximum at $H \simeq 150$ mT. The integral intensity of the scattering ($I_{\text{int}} = A_{\max} \kappa$) is equal within the error bars for all directions of the wave vector $\mathbf{q}$. It is constant at $H < 200$ mT, then it diminishes to zero at $H \simeq H_{c2}$. This type of behavior is observed in

the whole critical temperature range up to $T=T_c+0.8$ K. The value of the characteristic field $H\sim 150$ mT does not change but the absolute value of the effect for $\mathbf{q}\|\mathbf{H}\|[111]$ becomes less pronounced with increase of the temperature.

The data for configuration (ii) ($\mathbf{k}_0\|[11\bar{2}]$) were treated in the same way as for configuration (i). For $T=T_c+0.2$ K the q dependence of the scattering intensity along [111], [1$\bar{1}$0], and [201] axes are well fitted by the Lorentzian. The magnetic field dependence of the parameters obtained are presented in Figs. 9(a) and 9(b), respectively. As seen from Fig. 8(a), the inverse correlation length κ for $\mathbf{q}\|[201]$ does not change significantly with the magnetic field, similar to the behavior of κ along [001] axis in Fig. 8(a). For $\mathbf{q}\|\mathbf{H}\|[111]$ the change of κ, similar to that for configuration (i) [Fig. 8(a)], is observed. For $\mathbf{q}\|[1\bar{1}0]$ its value is constant for small H then it decreases in the range $130<H<180$ mT and practically coincides with that along [111] axis. For larger fields it increases again. The integral intensity of the scattering ($I_{\text{int}}=A_{\max}\kappa$) is of the same order for all directions of the wave vector $\mathbf{q}$ at small values of fields $H<200$ mT [Fig. 9(b)]. Then it diminishes to zero at different values of the field for different axes.

V. NATURE OF FIELD-INDUCED HELIX REORIENTATION IN MnSi

Thus, to summarize the experimental results: the magnetic structure of the MnSi is the left-handed helices oriented along four ⟨111⟩ axes. Four different domains coexist in the sample. The magnetic field, applied along the [111] axis, lifts the degeneracy of the magnetic system. The axis along the field becomes energetically more favorable as compared to the other three ⟨111⟩ axes. This single domain structure appears above the magnetic field H_{c1}, which in the critical range is of order of 30 mT. Further increase of the field leads to the 90° reorientation of the spin helix from the [111] axis (also the field axis) to [1$\bar{1}$0] axis in the field range from 130 to 180 mT. Reverse rotation occurs at $H>180$ mT. The helix transforms into the conical structure, which becomes the field-induced ferromagnet at $H_{c2}\simeq 350$ mT at $T=28.5$ K. This 90° rotation occurs in the close vicinity to T_c. Figure 10 shows the H-T phase diagram in the critical region. The lowest line on the diagram $H_{c1}(T)$ shows the transition from multidomain to the single domain helix structure. The upper line $H_{c2}(T)$ gives the transition from the conical to the ferromagnetic structure. Two lines between them $H_{R1}(T)$ and $H_{R2}(T)$ correspond to the 90° rotation of the helix wave vector $\mathbf{k}$ from the [111] axis to the [1$\bar{1}$0] axis and back, respectively. This rotation elucidates the nature of the so-called A phase observed by different techniques in Refs. 19 and 21. Our observation shows that no new A phase occurs. Instead we have dealt with the $\mathbf{k}$ rotation under applied field from one energetically favorable direction to the other.

We interpret the obtained data using a theoretical description recently developed by one of the authors (S.M.)[15] for cubic helical magnet with Dzyaloshinskii-Moriya interaction (DMI). To describe the properties of the system the following interactions were taken into account: conventional isotropic exchange, DM interaction, AE interaction, magnetic dipole interaction, Zeeman energy, and cubic anisotropy. The ground state energy in magnetic field and the spin wave spectrum were evaluated. It is well known that DMI is responsible for magnetic helix structure. In cubic crystals the DMI fixes the sense of the helix (right or left handed) but cannot determine its direction. It is stabilized by very weak AE interaction.[3–5] In Ref. 15 it was shown that in zero field the classical energy depends on the orientation of the helix vector $\mathbf{k}$. For three principal crystallographic directions the [111], [100], and [110] corresponding terms in the ground state energy are given by

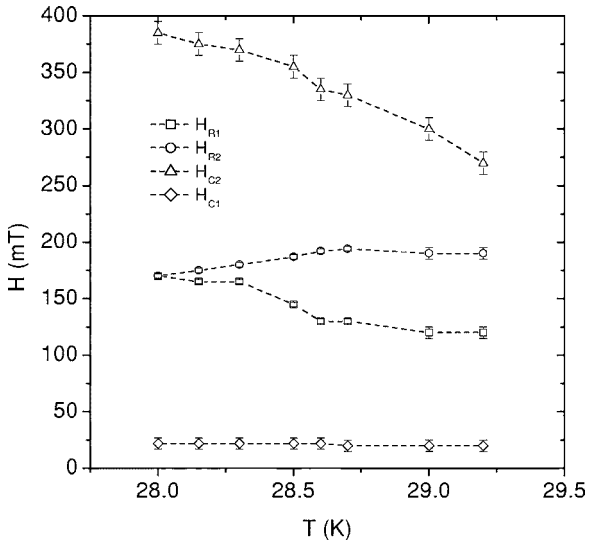

FIG. 10. H-T phase diagram of MnSi in the critical temperature range.

$$E_{cl[111]}=\frac{S^2Fk^2}{6}+\frac{S^4K}{2};$$

$$E_{cl[100]}=\frac{3S^4K}{4};\quad E_{cl[110]}=\frac{S^2Fk^2}{8}+\frac{9S^4K}{16}, \tag{5}$$

where F and K are the anisotropic exchange and the cubic anisotropy constants, respectively, and k is the helix wave vector. From these expressions we see that the helix structure along ⟨111⟩ is realized if $S^2Fk^2<3S^4K/2$. Otherwise, we have the ⟨100⟩ structure. The structure ⟨110⟩ is impossible as two conditions $E_{cl[111]}>E_{cl[110]}$ and $E_{cl[100]}>E_{cl[110]}$ contradict one another. Although these expressions are derived for $T=0$, the interplay between two anisotropy constants F and K must determine the helix direction for high temperatures as well. Indeed, Eqs. (5) are based solely on the cubic symmetry and have to be applicable near T_c also if one considers the constants F and K as functions of the reduced temperature $|\tau|=(T_c-T)/T_c$. Thus, we believe that Eqs. (5) give also anisotropic contribution for the free energy near T_c.

In the theory[15] the role of the spin wave gap Δ was discussed. It was shown that the gap determines behavior of the system in the case when the magnetic field perpendicular to the helix axis $\mathbf{k}$ is applied. In a weak field $g\mu_B H_\perp=h_\perp$

$<\Delta\sqrt{2}$ the direction of **k** is not sensitive to $h_\perp$. As soon as $h_\perp \simeq \Delta\sqrt{2}$ the helix axis rotates toward the field and establishes along the field at $h_\perp > \Delta\sqrt{2}$. It was shown also that there are two contributions to square of the gap value Δ^2. The first is a result of the spin-wave interaction and is independent on the **k** direction. The second is a result of the cubic anisotropy and for different directions of **k** is given by

$$\Delta^2_{cub[111]} = 4S^3Kh_c; \quad \Delta^2_{cub[100]} = 6S^3Kh_c;$$

$$\Delta^2_{cub[110]} = (9/2)S^3Kh_c, \tag{6}$$

where $h_c = g\mu H_{c2}$ is the critical field corresponding to the transition from helimagnetic state to the induced ferromagnetic state. It is seen that Δ^2_{cub} is positive for $K>0$ only. These expressions were derived in Ref. 15 at $T=0$ also, but may be used near T_c as the expressions [Eqs. (5)] for anisotropic part of the free energy.

In a weak perpendicular magnetic field $g\mu_B H_\perp < \Delta\sqrt{2}$ the helical spin structure becomes deformed. It is a result of Bose condensation of spin waves with momenta $\mathbf{q} = \pm\mathbf{k}$ and $\mathbf{q} = \mathbf{0}$.[15] As a result the second harmonic of the spin rotation with the wave vector **k** appears. It was observed in FeGe (Ref. 16) and MnSi.[17] The appearance of the perpendicular magnetic susceptibility was predicted too and the field dependent part of the free energy has the form

$$E_h = -\frac{Sh_\parallel^2}{2h_c} - \frac{Sh_\perp^2\Delta^2}{2h_c(1+\cos^2\alpha)[\Delta^2 - (h_\perp^2/2)\cos^4\alpha]}, \tag{7}$$

where $h_\parallel$ and $h_\perp$ are the components of the magnetic field h parallel and perpendicular to the helix wave vector **k**, and $\sin\alpha = -h_\parallel/h_c$ determines the cone angle of the helix in the external field. The first term of this expression is the magnetic part of the classical energy. It describes the interaction between the magnetic field projected onto the helix axis $h_\parallel$ and the mean spin induced by the field $S\sin\alpha = -Sh_\parallel/h_c$. The second term describes the interaction of the field, perpendicular to the helix vector, with the helix. In this expression Δ^2 depends on the **k** direction due to the cubic anisotropy [see Eq. (6)].

The real direction of the helix axis is determined by competition between the magnetic energy [Eq. (7)] and anisotropic energy given by Eq. (5). In our experiment the magnetic field is applied along the [111] axis and one can combine Eqs. (5) and (7) to write the expressions for the free energy near T_c for two orientations of the helix vector **k** along the [111] and $[1\bar{1}0]$:

$$E_{\mathbf{k}\|[\mathbf{111}]\|\mathbf{h}} = \frac{S^2Fk^2}{6} + \frac{S^4K}{2} - \frac{Sh^2}{2h_c};$$

$$E_{\mathbf{k}\|[\mathbf{1\bar{1}0}]\perp\mathbf{h}} = \frac{S^2Fk^2}{8} + \frac{9S^4K}{16} - \frac{Sh^2\Delta^2}{4h_c[\Delta^2 - (h^2/2)]}. \tag{8}$$

The ground free energy is presented in Fig. 11 as a function of the field for two possible orientations of the helix wave vector. We take the values of the free parameters close to the experimental conditions: the gap $\Delta = 80$ mT and the critical field $h_c = 340$ mT. It is seen from the figure that the energy

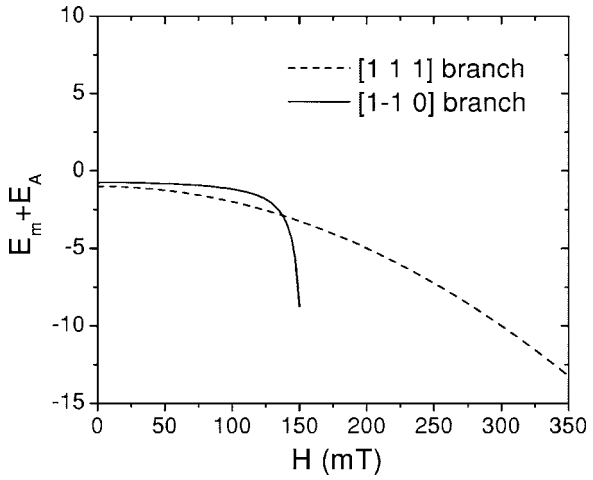

FIG. 11. The orientation dependent part of the free energy (sum of the anisotropic and the magnetic energies) as a function of the field for the helix axis along the field direction [111] and $[1\bar{1}0]$ for parameters $H_c = 340$ mT and $\Delta = 80$ mT.

branch corresponding to the $[1\bar{1}0]$ direction has a deep minimum in the field of order of 150 mT and becomes smaller than the branch corresponding to the [111] direction: $E_{\mathbf{k}\|[\mathbf{111}]\|\mathbf{h}} > E_{\mathbf{k}\|[\mathbf{1\bar{1}0}]\perp\mathbf{h}}$ for $H > 130$ mT. Indeed, if the field is along [111] the free energy decreases as soon as $h \to h_c$ according to the first line of Eqs. (8). Then at $h > h_c$ we have ferromagnetic spin configuration. However, the energy $E_{\mathbf{k}\|[1\bar{1}0]\perp\mathbf{h}}$, which corresponds to $[1\bar{1}0]$ orientation of the helix axis, decreases faster with the field growing and at the critical field determined by the condition $E_{\mathbf{k}\|[111]\|\mathbf{k}} = E_{\mathbf{k}\|[1\bar{1}0]\perp\mathbf{h}}$ and the first-order transition takes place with rotation of **k** along $[1\bar{1}0]$. This configuration remains stable up to $h \simeq \Delta_{[1\bar{1}0]}\sqrt{2}$. For larger h the $[1\bar{1}0]$ configuration is unstable, and the [111] configuration restored. It should be noted that the critical condition $h = \Delta\sqrt{2}$ is an approximate one as all corresponding expressions are not applicable if h approaches closely the critical value $\Delta\sqrt{2}$.

Thus we explain the observation of 90° rotation of the helix wave vector under applied field and this consideration is applicable for all $T < T_c$. On the contrary the helix reorientation is experimentally observed in the close vicinity to T_c. This may be understood bearing in mind that (i) the major contribution (interaction between spin waves) into the gap Δ is temperature independent and positive; (ii) the 90° rotation is solely caused by the interaction of the helix with the magnetic field and is proportional to S [Eqs. (7) and (8)]; (iii) the AE interaction and the cubic anisotropy are proportional to S^2 [Eq. (5)] and, therefore, are very weak in the critical range. It is clear that the magnetic energy prevails at the AE interaction and cubic anisotropy in the critical range while it is the other way around at low temperature.

VI. CONCLUSION

(i) We have investigated the appearance of a helix instability near T_c under applied field. The magnetic field produces magnetically single domain sample with the helix axis

parallel to the field. Further increase of the field results in the 90° rotation of the helix vector with respect to the field direction in a field range from 130 to 180 mT. The field above 180 mT restores the original orientation of the helix axis and leads to the induced ferromagnetic state at 340 mT. This **k**-rotation effect is observed over small temperature range near $T \simeq T_c$.

(ii) We explain the appearance of this phase within the theory recently developed for cubic helical magnet with DMI.[15] In this theory it is shown that the real direction of the helix axis is determined by the interplay between the magnetic energy, anisotropic exchange energy and cubic anisotropy. The phenomenon is a result of competition of cubic anisotropy and the spin-wave Bose condensation provoked by the field perpendicular to the helix axis.

ACKNOWLEDGMENTS

The PNPI teams acknowledge GKSS for hospitality. The authors are grateful to P. Böni for fruitful discussions and kind cooperation and to D. Solina for orientation of the sample. The Russian authors thank RFBR for partial support (Grant Nos. 04-02-16342 and 05-02-19889, 03-02-17340 and 00-15-96814) Russian Programs "Quantum macrophysics" and "Strongly correlated electrons in semiconductors, metals, superconductors and magnetic materials."

*Electronic address: grigor@pnpi.spb.ru

[1] Y. Ishikawa, K. Tajima, D. Bloch, and M. Roth, Solid State Commun. **19**, 525 (1976).
[2] Y. Ishikawa, G. Shirane, J. A. Tarvin, and M. Kohgi, Phys. Rev. B **16**, 4956 (1977).
[3] I. E. Dzyaloshinskii, Zh. Eksp. Teor. Fiz. **46**, 1420 (1964) [Sov. Phys. JETP **19**, 960 (1964)].
[4] P. Bak and M. H. Jensen, J. Phys. C **13**, L881 (1980).
[5] D. Nakamishi, A. Janase, A. Hasejawa, and M. Kitaoka, Solid State Commun. **35**, 995 (1980).
[6] M. Kataoka and O. Nakanishi, J. Phys. Soc. Jpn. **50**, 3888 (1981).
[7] C. Pfleiderer, G. J. McMullan, S. R. Julian, and G. G. Lonzarich, Phys. Rev. B **55**, 8330 (1997).
[8] C. Pfleiderer, S. R. Julian, and G. G. Lonzarich, Nature (London) **414**, 427 (2001).
[9] C. Pfleiderer, D. Resnik, L. Pintschovius, H. Von Lohneysen, M. Garst, and A. Rosch, Nature (London) **427**, 227 (2004).
[10] S. Sachdev, Rev. Mod. Phys. **75**, 913 (2003).
[11] V. Barzykin and L. P. Gorkov, Phys. Rev. Lett. **70**, 2479 (1993).
[12] K. Koyama, T. Goto, T. Kanomata, and R. Note, Phys. Rev. B **62**, 986 (2000).
[13] M. L. Plumer and M. B. Walker, J. Phys. C **14**, 4689 (1981).
[14] M. B. Walker, Phys. Rev. B **40**, 9315 (1989).
[15] S. V. Maleyev, Phys. Rev. B **73**, 174402 (2006).
[16] B. Lebech, J. Bernhard, and T. Frelthift, J. Phys.: Condens. Matter **1**, 6105 (1989).
[17] A. I. Okororkov, S. V. Grigoriev, Yu. O. Chetverikov, S. V. Maleyev, R. Georgii, B. Böni, D. Lamago, H. Eckerlebe, and P. K. Pranzas, Physica B **356**, 259 (2005).
[18] S. V. Grigoriev, S. V. Maleyev, A. I. Okorokov, Yu. O. Chetverikov, R. Georgii, P. Böni, D. Lamago, H. Eckerlebe, and K. Pranzas, Phys. Rev. B **72**, 134420 (2005).
[19] K. Kadowaki, K. Okuda, and M. Date, J. Phys. Soc. Jpn. **51**, 2433 (1982).
[20] Y. Ishikawa and M. Arai, J. Phys. Soc. Jpn. **53**, 2726 (1984).
[21] C. Thessieu, C. Pfleiderer, A. N. Stepanov, and J. Flouquet, J. Phys.: Condens. Matter **9**, 6677 (1997).
[22] S. V. Maleyev, V. G. Bar'jakhtar, and R. A. Suris, Fiz. Tverd. Tela (S.-Peterburg) **4**, 3461 (1962).
[23] M. Blume, Phys. Rev. **130**, 1670 (1963).